Research Article Vol. 31, No. 2 / 16 Jan 2023 / Optics Express 3315
Optics EXPRESS

Single and multi-pulse based X-ray photon correlation spectroscopy

WONHYUK JO,[1,2,6,*] STEPHAN STERN,[3] FABIAN WESTERMEIER,[1] RUSTAM RYSOV,[1] MATTHIAS RIEPP,[1,4] JULIAN SCHMEHR,[3] JÖRN LANGE,[3] JULIAN BECKER,[3] MICHAEL SPRUNG,[1] TORSTEN LAURUS,[1] HEINZ GRAAFSMA,[1] IRINA LOKTEVA,[1,5] GERHARD GRÜBEL,[1,2,5] AND WOJCIECH ROSEKER[1,7]

[1]*Deutsches Elektronen-Synchrotron DESY, Notkestr. 85, 22607 Hamburg, Germany*
[2]*Present address: European X-ray Free Electron Laser GmbH, Holzkoppel 4, 22869, Schenefeld, Germany*
[3]*X-Spectrum GmbH, Luruper Hauptstr. 1, 22547 Hamburg, Germany*
[4]*Present address: Université de Strasbourg, CNRS, Institut de Physique et Chimie des Matériaux de Strasbourg, UMR 7504, F-67000 Strasbourg, France*
[5]*The Hamburg Centre for Ultrafast Imaging, Luruper Chaussee 149, 22761 Hamburg, Germany*
[6]*wonhyuk.jo@xfel.eu*
[7]*wojciech.roseker@desy.de*
[*]*wins1119@gmail.com*

Abstract: The ability of pulsed nature of synchrotron radiation opens up the possibility of studying microsecond dynamics in complex materials via speckle-based techniques. Here, we present the study of measuring the dynamics of a colloidal system by combining single and multiple X-ray pulses of a storage ring. In addition, we apply speckle correlation techniques at various pulse patterns to collect correlation functions from nanoseconds to milliseconds. The obtained sample dynamics from all correlation techniques at different pulse patterns are in very good agreement with the expected dynamics of Brownian motions of silica nanoparticles in water. Our study will pave the way for future pulsed X-ray investigations at various synchrotron X-ray sources using individual X-ray pulse patterns.

1. Introduction

Speckle-based techniques are well established to investigate sample dynamics in soft matter. The high coherence beam leaves an imprint of the spatial distribution of the subjected system on a diffraction image as a grainy interference pattern at the detector plane, which is typically called "speckle". The movement of disordered particles shifts the relative phases of the scattered field and induces temporal variations in the speckle patterns. Consequently, these fluctuating speckle intensities reflect the information of the system dynamics, which can be quantified by a correlation function. For many decades, optical laser systems have been widely employed to generate speckle patterns for photon correlation spectroscopy (PCS) [1–3]. Thanks to the improvement of the coherent X-ray flux from synchrotron sources, X-rays have been employed for speckle-based measurements of dynamics on the atomic scale [4] or optically turbid system [5].

One of the most robust techniques, called X-ray photon correlation spectroscopy (XPCS), is a powerful and convenient tool for measuring dynamics. The temporal resolution of the technique is defined by the number of images taken in time. In the past decades, considerably slow systems have been in the focus of XPCS studies [6–14]. Recently, new advanced detector technology has begun to offer 2D detectors with the microsecond temporal resolutions in XPCS measurements (e.g., VIPIC [15], UFXC32k [16], Tristan detector [17], and the XSPA-500k [18]). Recently developed X-ray detectors offering MHz frame rates, such as adaptive gain integrated pixel detector (AGIPD), enable to investigate of nanosecond colloidal dynamics at 3rd generation

#477774 https://doi.org/10.1364/OE.477774
Journal © 2023 Received 12 Oct 2022; revised 9 Dec 2022; accepted 13 Dec 2022; published 13 Jan 2023

Optics EXPRESS

X-ray synchrotron sources [19] and X-ray free electron laser (XFEL) sources [20,21]. In order to measure sample dynamics faster than accessible with XPCS, X-ray speckle visibility spectroscopy (XSVS) has been developed, which evaluates a speckle contrast as a function of illumination time. The longer illumination time compared to system dynamics leads the more blurred speckle images and a loss in contrast of the speckle images. This concept was introduced in optical laser systems [22] and extended to X-ray regime [23–27].

An alternative speckle technique is double pulse XPCS (DP-XPCS). The technique evaluates a speckle contrast of two summed speckle patterns separated with a delay time, which corresponds to the temporal resolution. DP-XPCS has been demonstrated with sequentially obtained speckle patterns [28] and an optical pulse laser scheme [29]. More recently, DP-XPCS has been employed in a special operation mode of linear accelerators of XFEL [30,31] or X-ray split-and-delay unit [32–42] to investigate nanosecond dynamics beyond detector frame rate limitations.

In this paper, we demonstrated XPCS measurements using single and multiple X-ray pulses from nanoseconds to milliseconds time scales. Thanks to the MHz frame rate of the detector, we investigated the sample dynamics with 192 ns temporal resolution in a single pulse mode. In addition, we covered the gap between nanoseconds to milliseconds using the multiple X-ray pulse modes in the correlation function. The obtained sample dynamics are in excellent agreement with the expected dynamics of the system.

2. Materials and methods

2.1. Experiments

The experiment was conducted at the coherent application beamline P10 of PETRA III [43]. The monochromatic 8 keV X-ray beam was focused vertically and horizontally down to d_b = 2.5 μm at the sample position. The speckle size d_s = 310 μm was estimated at the detector plane located at a distance L = 5 m, according to $d_s = \lambda L/d_b$, where λ is the X-ray wavelength. The silica colloidal nanoparticles (NPs) with a core radius R of 65 nm were dispersed in water and filled in a 700 μm thick quartz capillary. The SPARTA detector, which was developed by the X-Spectrum GmbH with AGIPD technology [44–46] was employed to measure the sample dynamics. The detector is composed of 128 × 512 pixels with a pixel size of 200 μm × 200 μm. It can collect up to 352 memory cells (i.e., frames) at a frame rate in the MHz range in a single burst (i.e., measurement). The images have to be read out until the next MHz acquisition burst can be triggered 0.1 s later. Note that the number of X-ray pulses (N) between two consecutive frames adjusts the time resolution and the achievable time window in correlation functions. In this work, we selected N = 1, 5, and 40 to capture the sample dynamics (see Supplement 1 and Table 1). The detector signal was carefully extracted using a background subtraction method that is elaborated elsewhere [19,21] and subsequent conversion of the cleaned signal to an integer number of photons. An additional pixel mask was applied in the analysis to exclude detector pixels with high electronic noise. The depicted speckle patterns after the data conversion process to photons are shown in Fig. 1(b).

Table 1. Data collection modes of SPARTA. *N* and Δt denote the number of X-ray pulses between two successive frames and the time range of correlation functions, respectively.

N	Δt
1 (N_1, Single pulse mode)	192 ns - 67.6 μs
5 (N_5, 5 pulse mode)	960 ns - 338 μs
40 (N_{40}, Revolution mode)	7.68 μs - 2.7 ms

Optics EXPRESS

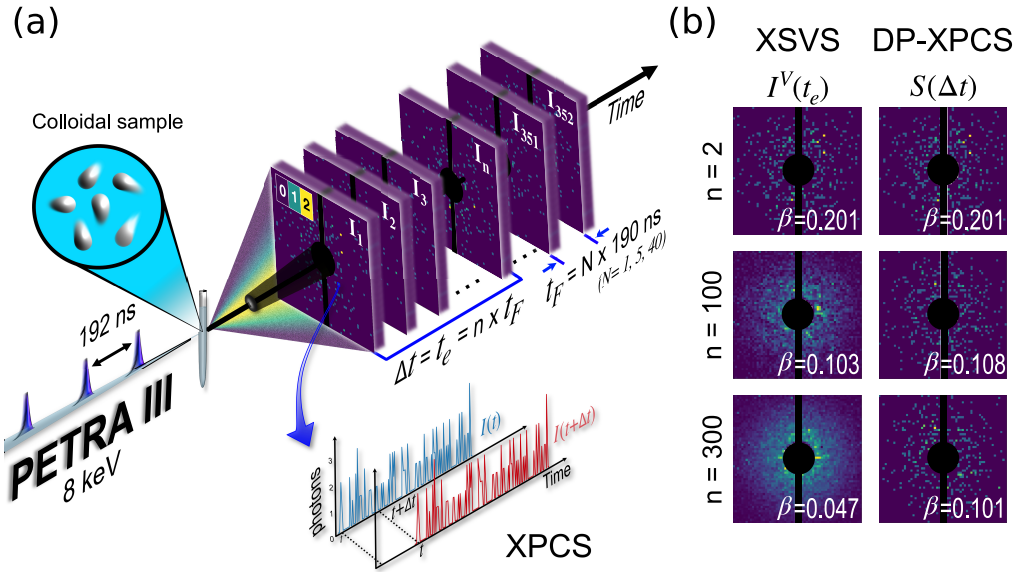

Fig. 1. (a) Schematics of the speckle measurement experiment employing the intrinsic pulse structure of PETRA III. Coherent X-ray pulses are delivered at the sample position with 192 ns temporal separation. SPARTA collects 352 images in a single measurement, and the delay time between each frame is set by the number of X-ray pulses between two consecutive frames N. (b) Speckle images of XSVS and DP-XPCS for N_{40} with varying number of frames n.

2.2. X-ray photon correlation spectroscopy

Three complementary XPCS techniques (i.e., XPCS, XSVS, and DP-XPCS) were employed to evaluate the sample dynamics obtained from different collection modes.

2.2.1. XPCS

The intensity fluctuations in time are caused by the spatial rearrangement of colloidal particles. The sample dynamic properties are traced by the intensity autocorrelation function together with the Siegert relation [47,48]

$$g^{(2)}(Q,\Delta t) = \frac{\langle I(Q,t)I(Q,t+\Delta t)\rangle}{\langle I(Q,t)\rangle^2} = 1 + \beta_0 |f(Q,\Delta t)|^2, \tag{1}$$

where $I(Q,t)$ denotes the intensity of the speckle pattern at wavevector Q and time t. The bracket $\langle\rangle$ stands for time averaging, and Δt represents a delay time. The wavevector Q is defined by λ and scattering angle 2θ according to $Q = 4\pi \sin(\theta)/\lambda$. The β_0 is the speckle contrast mostly defined by the degree of coherence of the beam and experimental configuration [49,50]. For the simple monodisperse colloidal case, the intermediate scattering function (ISF: $f(Q,\Delta t)$) is considered via a simple exponential decay function

$$f(Q,\Delta t) = \exp(-\Gamma(Q)\Delta t), \tag{2}$$

where $\Gamma(Q) = D_0 Q^2$ for typical Brownian motion and D_0 is defined by the Stokes-Einstein relation as $D_0 = \frac{k_b T}{6\pi\eta R}$, where k_b, T, η are the Boltzmann constant, environment temperature and medium viscosity, respectively. Note that in the limit of $\Delta t \to 0$, the $g^{(2)} - 1$ corresponds to the

Optics EXPRESS

$\beta_0(\Delta t = 0)$ and decreases as a function of Δt taking into account the sample dynamics that can be expressed as

$$\beta_0 \exp(-2\Gamma\Delta t) = g^{(2)}(Q, \Delta t) - 1. \tag{3}$$

The obtained correlation function provides the contrast $\beta^C(Q, \Delta t) = \beta_0 \exp(-2\Gamma(Q)\Delta t)$ that starts with β_0 and decreases as a function of Δt due to the sample dynamics.

2.2.2. X-ray speckle visibility spectroscopy

In order to investigate system dynamics using XSVS from sequentially obtained speckle patterns, a speckle image with an exposure time t_e is defined as $I^V(Q, t_e) = \int_t^{t+t_e} I(Q, t')dt' = \sum_n^{n+n_e} I(Q, n)$, where $t_e = 190$ ns $\times n_e N$, and n_e is the number of frames corresponding to t_e. The extending of t_e does not affect the speckle contrast until the sample characteristic time Γ^{-1} is sufficiently smaller than t_e. In contrast, when $t_e > \Gamma^{-1}$, the speckle image is washed out, and consequently, the contrast decreases. In Fig. 1(b), the degrading of speckle image clarity as a function of n is clearly observed, and the normalized variance $\beta \equiv M^{-1} = \sigma^2(I^V)/\langle I^V \rangle^2$, where M is a number of speckle mode in the intensity is given by [22,51,52]

$$\beta_V(Q, \Delta t) = \frac{2\beta_0}{t_e} \int_0^{t_e} (1 - t/t_e)|f(Q, \Delta t)|^2 dt. \tag{4}$$

In case of the simple exponential decay function $f(Q, \Delta t) = \exp(-\Gamma\Delta t)$, Eq. (4) can be solved analytically as

$$\beta_V(Q, \Delta t) = \frac{\beta_0}{2\Gamma^2 t_e^2}[2\Gamma t_e - 1 + \exp(-2\Gamma t_e)]. \tag{5}$$

Note that the Eq. (5) shows more moderate decay in contrast compared to the β^C.

2.2.3. Double pulse XPCS

Double pulse speckle contrast β from the sum of two speckle patterns $S(Q, \Delta t) = I(Q, t) + I(Q, t+\Delta t)$ enables to quantify the level of displacements of colloidal particles within the delay time Δt. The contrast is given by the normalized variance of intensity distribution at a wavevector Q evaluated as [28]

$$\begin{aligned} c_2(Q, \Delta t) &= \frac{\langle S^2(Q, \Delta t)\rangle - \langle S(Q, \Delta t)\rangle^2}{\langle S(Q, \Delta t)\rangle^2} \\ &= \frac{\beta_0}{2}(1 + |f(Q, \Delta t)|^2) + \alpha, \end{aligned} \tag{6}$$

where α is the shot noise.

For weak speckle patterns, the photon counting statistics should be accounted for. The probability distribution of the number of photons per pixel k in a speckle pattern is described by the negative binomial distribution function [53]

$$P_{NB}(k) = \frac{\Gamma(k + M)}{\Gamma(M)\Gamma(k + 1)} \left(1 + \frac{M}{\langle k\rangle}\right)^{-k} \left(1 + \frac{\langle k\rangle}{M}\right)^{-M}. \tag{7}$$

In the negative binomial distribution, the normalized variance can be expressed as $M^{-1} = \sigma^2(k)/\langle k\rangle^2 - 1/\langle k\rangle$ [4].

3. Result and discussion

Figure 2(a) shows the averaged intensity collected at the N_1, N_5, and N_{40}, respectively. A total of 4700 bursts were employed to obtain a sufficient signal-to-noise ratio for N_1 and N_5, and 470 bursts were used for N_{40}. The azimuthally integrated intensity profiles are shown in Fig. 2(b).

Optics EXPRESS

The intensity profiles fall off as a function of Q. The particle formfactor ring is well pronounced at $Q = 0.09$ nm^{-1} for N_{40}, indicating a system of sufficiently dilute and non-interacting silica particles. A single-sphere formfactor fit to the intensity profile obtained with N_{40} yields $R = 65.2\pm0.3$ nm and size polydispersity $\Delta R/R = 7.41$ %.

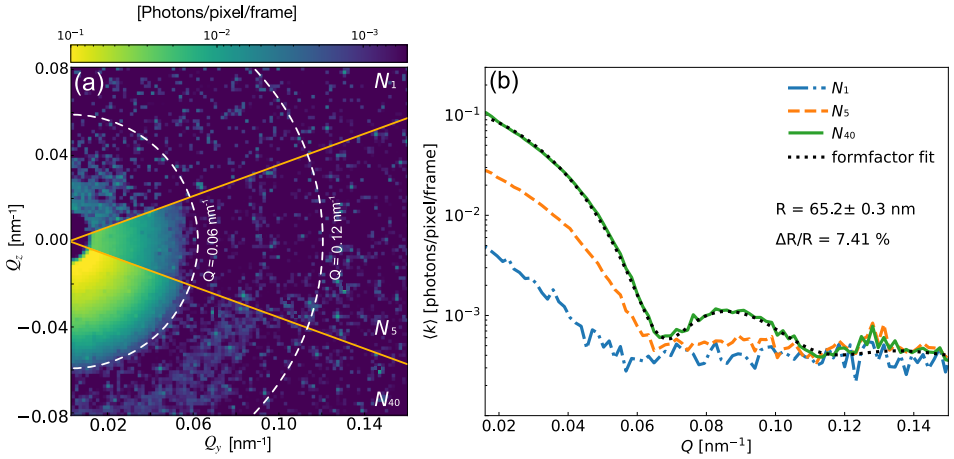

Fig. 2. (a) 2D speckle pattern taken by SPARTA for N_1, N_5, and N_{40}. (b) Corresponding azimuthally integrated intensity profiles as a function of Q. The black dotted line represents the formfactor fit, taking into account the sample polydispersity ($\Delta R/R$).

We divided the detector plane into regions of interest (ROI) that are limited by contours of equivalent wavevector Q for further analysis.

Figure 3 shows $g^{(2)}$ obtained from N_1, N_5, and N_{40} using Eq. (1). The dashed lines represent expected dynamics according to Eq. (3) where the initial contrast at $\Delta t \rightarrow 0$ is $\beta_0 = 0.2$. A considerably larger error in N_1 is due to the lower photon count rates. Nevertheless, resolving a single X-ray pulse in XPCS offers a 192 ns temporal resolution in this pulse pattern [19].

Figure 4 shows a square of ISF obtained from XPCS ($g^{(2)}$: filled markers) and DP-XPCS ($c^{(2)}$: empty markers) in N_{40} for various Q values. The ISF from $g^{(2)}$ extracted from Eq. (1) decays as a function of delay time representing the motion of silica particles. The obtained initial contrast β_0 from $g^{(2)}$ was employed to Eq. (6) to extract ISF and α from $c^{(2)}$. The black dashed lines represent dynamics of Brownian motion in freely diffusing silica particles in water with the relaxation rate Γ of 1315, 2578, and 4262 s^{-1} at $Q = 0.02$, 0.028, and 0.037 nm^{-1}, respectively.

We calculated speckle contrast as a function of exposure time to obtain the X-ray speckle visibility using the normalized variance. In contrast to the XPCS and DP-XPCS, the image $I^V(Q, t_e)$ for XSVS is a result of the summation of all the memory cells between the corresponding delay time. Figure 5 shows speckle visibility contrast as red squares for $Q = 0.02$ (a), 0.028 (b), and 0.037 (c), respectively. Also, XPCS results are shown as blue circles at corresponding Q in N_{40}. The dotted and dashed lines for the XPCS and XSVS experiment are the fit using Eq. (3) and Eq. (5), respectively. The extracted Γ as a function of wavevector transfer is in excellent agreement for all three approaches in Fig. 6. This result shows that all the methods are well suited for pulsed-based studies.

Dynamics measured via pulsed-based XPCS in a model colloidal model system of silica particles in water mark an important step in adopting various pulse patterns of storage rings in XPCS measurements. A higher coherent flux available with diffraction-limited storage rings (DLSR) will extend the access to study weakly scattering, but very relevant systems [54]. The possibility of employing a time structure of DLSRs paves the way to studying dynamics on nanosecond to microsecond timescales bridging the experimental gap between 3rd generation

Optics EXPRESS

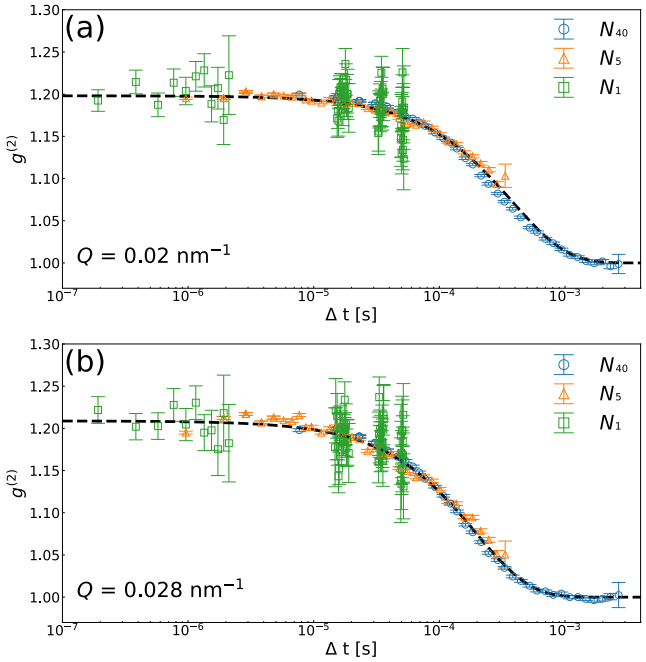

Fig. 3. Intensity correlation functions as a function of delay time obtained from N_1 (green-square), N_5 (orange-triangle), and N_{40} (blue-circle) for Q = 0.02 nm^{-1} (a) and 0.028 nm^{-1} (b). The dashed lines indicate the expected correlation functions using Eq. (3).

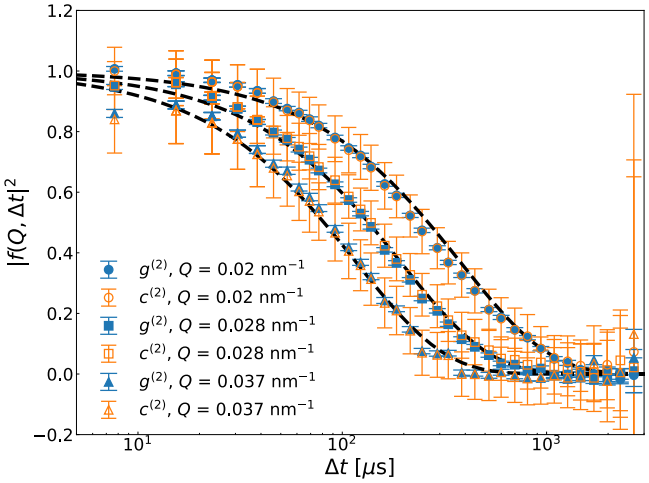

Fig. 4. The obtained intermediate scattering functions from XPCS (circle) and DP-XPCS (square) for varying Q. The black dashed lines represent the expected curves of a single exponential decay curve from Eq. (2).

Optics EXPRESS

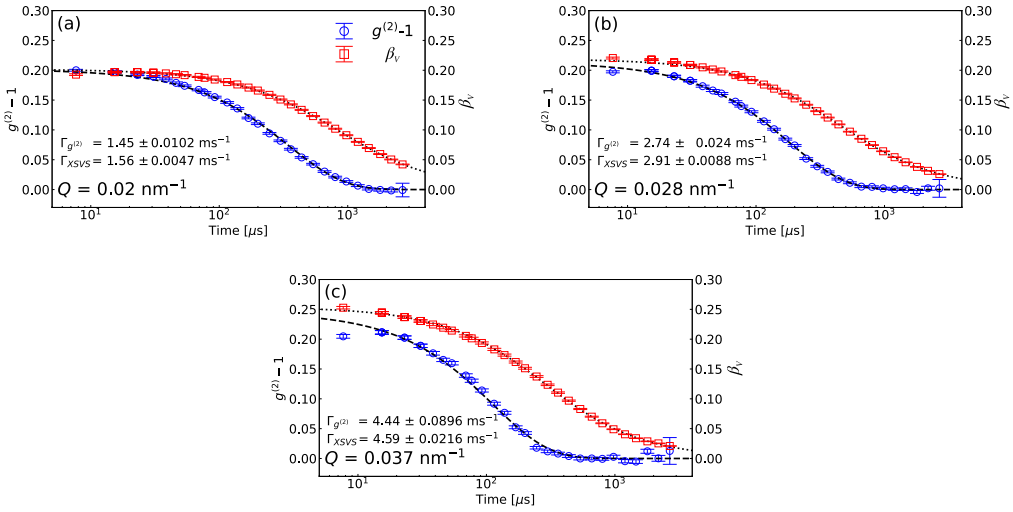

Fig. 5. Combined XPCS $g^{(2)}$-1 and speckle visibility contrast β_V at the wavevector transfer Q of (a) 0.02 nm^{-1}, (b) 0.028 nm^{-1}, (c) 0.037 nm^{-1}. The dashed and dotted lines are the fit result using Eq. (3) and Eq. (5), respectively.

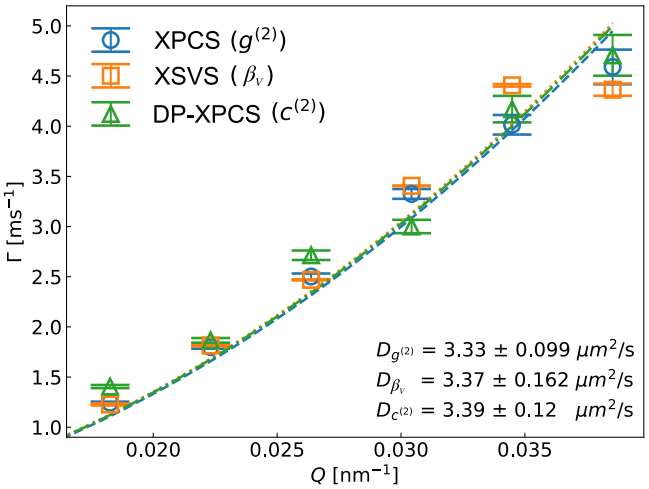

Fig. 6. Extracted Γ as a function of Q. The lines are the fitting results using $\Gamma(Q) = D_0 Q^2$.

Optics EXPRESS

synchrotron sources and XFEL sources in investigating more complex systems, in particular, fast relaxation processes in glasses [11], atomic diffusion in metal alloys [55], soft matter [20] and biological systems [56].

4. Conclusions

We have demonstrated pulsed XPCS at a synchrotron source by employing various pulse patterns of PETRA III. The diffusion coefficients obtained from the three speckle correlation techniques, i.e., XPCS, XSVS, and DP-XPCS, show very good agreement with the expected dynamics of the colloidal system. The SPARTA detector capability of MHz frame rates has provided a way of conducting such experiments with very short time resolutions, spanning the range from 190 ns over microseconds to milliseconds to cover a fast but also wide range of times in correlation functions. These studies will provide great potential for X-ray speckle-based investigation for all synchrotron facilities operated by individual X-ray repetition rates and, in particular, diffraction-limited storage rings.

Funding. Deutsche Forschungsgemeinschaft (SFB 925 170620586.) Cluster of Excellence "CUI: The Hanburg Centre for Ultrafast Imaging," (ECX 1074 194651731), Cluster of Excellence "CUI: Advanced Imaging of Matter," (EXC 2056 390715994); Hamburgishe Investitions und Forderbank (IFB); XSpectrum GmbH (51090010.);

Disclosures. The authors declare no conflicts of interest.

Data availability. Data underlying the results presented in this paper are not publicly available at this time but may be obtained from the authors upon reasonable request.

Supplemental document. See Supplement 1 for supporting content.

References

1. B. J. Berne and R. Pecora, *Dynamic Light Scattering* (John Wiley, New York, 1976).
2. D. K. Carpenter, "Dynamic light scattering with applications to chemistry, biology, and physics," J. Chem. Educ. **54**(10), A430 (1977).
3. P. Zakharov, S. Bhat, P. Schurtenberger, and F. Scheffold, "Multiple-scattering suppression in dynamic light scattering based on a digital camera detection scheme," Appl. Opt. **45**(8), 1756 (2006).
4. S. O. Hruszkewycz, M. Sutton, P. H. Fuoss, B. Adams, S. Rosenkranz, K. F. Ludwig, W. Roseker, D. Fritz, M. Cammarata, D. Zhu, S. Lee, H. Lemke, C. Gutt, A. Robert, G. Grübel, and G. B. Stephenson, "High contrast x-ray speckle from atomic-scale order in liquids and glasses," Phys. Rev. Lett. **109**(18), 185502 (2012).
5. E. F. Semeraro, J. Möller, and T. Narayanan, "Multiple-scattering effects in SAXS and XPCS measurements in the ultra-small-angle region," J. Appl. Crystallogr. **51**(3), 706–713 (2018).
6. S. B. Dierker, R. Pindak, R. M. Fleming, I. K. Robinson, and L. Berman, "X-Ray Photon Correlation Spectroscopy Study of Brownian Motion of Gold Colloids in Glycerol," Phys. Rev. Lett. **75**(3), 449–452 (1995).
7. G. Grübel and F. Zontone, "Correlation spectroscopy with coherent x-rays," J. Alloys Compd. **362**(1-2), 3–11 (2004).
8. F. Lehmkühler, J. Valerio, D. Sheyfer, W. Roseker, M. A. Schroer, B. Fischer, K. Tono, M. Yabashi, T. Ishikawa, and G. Grübel, "Dynamics of soft nanoparticle suspensions at hard X-ray FEL sources below the radiation-damage threshold," IUCrJ **5**(6), 801–807 (2018).
9. L. Frenzel, F. Lehmkühler, I. Lokteva, S. Narayanan, M. Sprung, and G. Grübel, "Anomalous Dynamics of Concentrated Silica-PNIPAm Nanogels," J. Phys. Chem. Lett. **10**(17), 5231–5236 (2019).
10. C. Gutt, T. Ghaderi, V. Chamard, A. Madsen, T. Seydel, M. Tolan, M. Sprung, G. Grübel, and S. K. Sinha, "Observation of Heterodyne Mixing in Surface X-Ray Photon Correlation Spectroscopy Experiments," Phys. Rev. Lett. **91**(7), 076104 (2003).
11. B. Ruta, Y. Chushkin, G. Monaco, L. Cipelletti, E. Pineda, P. Bruna, V. M. Giordano, and M. Gonzalez-Silveira, "Atomic-scale relaxation dynamics and aging in a metallic glass probed by X-ray photon correlation spectroscopy," Phys. Rev. Lett. **109**(16), 165701 (2012).
12. Z. Evenson, B. Ruta, S. Hechler, M. Stolpe, E. Pineda, I. Gallino, and R. Busch, "X-Ray Photon Correlation Spectroscopy Reveals Intermittent Aging Dynamics in a Metallic Glass," Phys. Rev. Lett. **115**(17), 175701 (2015).
13. Y. Chushkin, C. Caronna, and A. Madsen, "A novel event correlation scheme for X-ray photon correlation spectroscopy," J. Appl. Crystallogr. **45**(4), 807–813 (2012).
14. F. Perakis, K. Amann-Winkel, F. Lehmkühler, M. Sprung, D. Mariedahl, J. A. Sellberg, H. Pathak, A. Späh, F. Cavalca, D. Schlesinger, A. Ricci, A. Jain, B. Massani, F. Aubree, C. J. Benmore, T. Loerting, G. Grübel, L. G. M. Pettersson, and A. Nilsson, "Diffusive dynamics during the high-to-low density transition in amorphous ice," Proc. Natl. Acad. Sci. **114**(31), 8193–8198 (2017).

Optics EXPRESS

15. A. K. Rumaiz, D. P. Siddons, G. Deptuch, P. Maj, A. J. Kuczewski, G. A. Carini, S. Narayanan, E. M. Dufresne, A. Sandy, R. Bradford, A. Fluerasu, and M. Sutton, "First experimental feasibility study of VIPIC: a custom-made detector for X-ray speckle measurements," J. Synchrotron Radiat. **23**(2), 404–409 (2016).
16. Q. Zhang, E. M. Dufresne, S. Narayanan, P. Maj, A. Koziol, R. Szczygiel, P. Grybos, M. Sutton, and A. R. Sandy, "Sub-microsecond-resolved multi-speckle X-ray photon correlation spectroscopy with a pixel array detector," J. Synchrotron Radiat. **25**(5), 1408–1416 (2018).
17. S. Berkowicz, S. Das, M. Reiser, M. Filianina, M. Bin, G. Crevatin, F. Hennies, C. Weninger, A. Björling, P. Bell, and F. Perakis, "Nanofocused x-ray photon correlation spectroscopy," Phys. Rev. Res. **4**(3), L032012 (2022).
18. K. Switalski, J. Fan, L. Li, M. Chu, E. Sarnello, P. Jemian, T. Li, Q. Wang, and Q. Zhang, "Direct measurement of stokes-einstein diffusion of cowpea mosaic virus with 19 µs-resolved xpcs," J. Synchrotron Radiat. **29**(6), 1429–1435 (2022).
19. W. Jo, F. Westermeier, R. Rysov, O. Leupold, F. Schulz, S. Tober, V. Markmann, M. Sprung, A. Ricci, T. Laurus, A. Aschkan, A. Klyuev, U. Trunk, H. Graafsma, G. Grübel, and W. Roseker, "Nanosecond X-ray photon correlation spectroscopy using pulse time structure of a storage-ring source," IUCrJ **8**(1), 124–130 (2021).
20. F. Lehmkühler, F. Dallari, A. Jain, M. Sikorski, J. Möller, L. Frenzel, I. Lokteva, G. Mills, M. Walther, H. Sinn, F. Schulz, M. Dartsch, V. Markmann, R. Bean, Y. Kim, P. Vagovic, A. Madsen, A. P. Mancuso, and G. Grübel, "Emergence of anomalous dynamics in soft matter probed at the european xfel," Proc. Natl. Acad. Sci. **117**(39), 24110–24116 (2020).
21. F. Dallari, M. Reiser, I. Lokteva, A. Jain, J. Möller, M. Scholz, A. Madsen, G. Grübel, F. Perakis, and F. Lehmkühler, "Analysis strategies for mhz xpcs at the european xfel," Appl. Sci. **11**(17), 8037 (2021).
22. R. Bandyopadhyay, A. S. Gittings, S. S. Suh, P. K. Dixon, and D. J. Durian, "Speckle-visibility spectroscopy: A tool to study time-varying dynamics," Rev. Sci. Instrum. **76**(9), 093110 (2005).
23. I. Inoue, Y. Shinohara, A. Watanabe, and Y. Amemiya, "Effect of shot noise on x-ray speckle visibility spectroscopy," Opt. Express **20**(24), 26878–26887 (2012).
24. L. Li, P. Kwaśniewski, D. Orsi, L. Wiegart, L. Cristofolini, C. Caronna, and A. Fluerasu, "Photon statistics and speckle visibility spectroscopy with partially coherent X-rays," J. Synchrotron Radiat. **21**(6), 1288–1295 (2014).
25. F. Perakis, G. Camisasca, T. J. Lane, A. Späh, K. T. Wikfeldt, J. A. Sellberg, F. Lehmkühler, H. Pathak, K. H. Kim, K. Amann-Winkel, S. Schreck, S. Song, T. Sato, M. Sikorski, A. Eilert, T. McQueen, H. Ogasawara, D. Nordlund, W. Roseker, J. Koralek, S. Nelson, P. Hart, R. Alonso-Mori, Y. Feng, D. Zhu, A. Robert, G. Grübel, L. G. M. Pettersson, and A. Nilsson, "Coherent X-rays reveal the influence of cage effects on ultrafast water dynamics," Nat. Commun. **9**(1), 1917 (2018).
26. J. Möller, M. Reiser, J. Hallmann, U. Boesenberg, A. Zozulya, H. Rahmann, A.-L. Becker, F. Westermeier, T. Zinn, F. Zontone, C. Gutt, and A. Madsen, "Implications of disturbed photon-counting statistics of Eiger detectors for X-ray speckle visibility experiments," J. Synchrotron Radiat. **26**(5), 1705–1715 (2019).
27. J. Möller, M. Reiser, J. Hallmann, U. Boesenberg, A. Zozulya, H. Rahmann, A.-L. Becker, F. Westermeier, T. Zinn, M. Sprung, T. Narayanan, C. Gutt, and A. Madsen, "Using low dose x-ray speckle visibility spectroscopy to study dynamics of soft matter samples," New J. Phys. **23**(9), 093041 (2021).
28. C. Gutt, L.-M. Stadler, A. Duri, T. Autenrieth, O. Leupold, Y. Chushkin, and G. Grübel, "Measuring temporal speckle correlations at ultrafast x-ray sources," Opt. Express **17**(1), 55–61 (2009).
29. S. Lee, W. Jo, H. S. Wi, C. Gutt, and G. W. Lee, "Resolving high-speed colloidal dynamics beyond detector response time via two pulse speckle contrast correlation," Opt. Express **22**(18), 21567–21576 (2014).
30. M. H. Seaberg, B. Holladay, J. C. T. Lee, M. Sikorski, A. H. Reid, S. A. Montoya, G. L. Dakovski, J. D. Koralek, G. Coslovich, S. Moeller, W. F. Schlotter, R. Streubel, S. D. Kevan, P. Fischer, E. E. Fullerton, J. L. Turner, F.-J. Decker, S. K. Sinha, S. Roy, and J. J. Turner, "Nanosecond x-ray photon correlation spectroscopy on magnetic skyrmions," Phys. Rev. Lett. **119**(6), 067403 (2017).
31. Y. Sun, F.-J. Decker, J. Turner, S. Song, A. Robert, and D. Zhu, "Pulse intensity characterization of the LCLS nanosecond double-bunch mode of operation," J. Synchrotron Radiat. **25**(3), 642–649 (2018).
32. W. Roseker, H. Franz, H. Schulte-Schrepping, A. Ehnes, O. Leupold, F. Zontone, A. Robert, and G. Grübel, "Performance of a picosecond x-ray delay line unit at 8.39 kev," Opt. Lett. **34**(12), 1768–1770 (2009).
33. W. Roseker, H. Franz, H. Schulte-Schrepping, A. Ehnes, O. Leupold, F. Zontone, S. Lee, A. Robert, and G. Grübel, "Development of a hard X-ray delay line for X-ray photon correlation spectroscopy and jitter-free pump–probe experiments at X-ray free-electron laser sources," J. Synchrotron Radiat. **18**(3), 481–491 (2011).
34. W. Roseker, S. O. Hruszkewycz, F. Lehmkühler, M. Walther, H. Schulte-Schrepping, S. Lee, T. Osaka, L. Strüder, R. Hartmann, M. Sikorski, S. Song, A. Robert, P. H. Fuoss, M. Sutton, G. B. Stephenson, and G. Grübel, "Towards ultrafast dynamics with split-pulse x-ray photon correlation spectroscopy at free electron laser sources," Nat. Commun. **9**(1), 1704 (2018).
35. Y. Sun, M. Dunne, P. Fuoss, A. Robert, D. Zhu, T. Osaka, M. Yabashi, and M. Sutton, "Realizing split-pulse x-ray photon correlation spectroscopy to measure ultrafast dynamics in complex matter," Phys. Rev. Res. **2**(2), 023099 (2020).
36. J. Sakamoto, K. Ohwada, M. Ishino, J. Mizuki, M. Ando, and K. Namikawa, "Design of a prototype split-and-delay unit for XFEL pulses, and their evaluation by synchrotron radiation X-rays," J. Synchrotron Radiat. **24**(1), 95–102 (2017).

Optics EXPRESS

37. W. Lu, T. Noll, T. Roth, I. Agapov, G. Geloni, M. Holler, J. Hallmann, G. Ansaldi, S. Eisebitt, and A. Madsen, "Design and throughput simulations of a hard x-ray split and delay line for the mid station at the european xfel," AIP Conf. Proc. **1741**, 030010 (2016).
38. W. Lu, B. Friedrich, T. Noll, K. Zhou, J. Hallmann, G. Ansaldi, T. Roth, S. Serkez, G. Geloni, A. Madsen, and S. Eisebitt, "Development of a hard x-ray split-and-delay line and performance simulations for two-color pump-probe experiments at the european xfel," Rev. Sci. Instrum. **89**(6), 063121 (2018).
39. T. Hirano, T. Osaka, Y. Morioka, Y. Sano, Y. Inubushi, T. Togashi, I. Inoue, S. Matsuyama, K. Tono, A. Robert, J. B. Hastings, K. Yamauchi, and M. Yabashi, "Performance of a hard X-ray split-and-delay optical system with a wavefront division," J. Synchrotron Radiat. **25**(1), 20–25 (2018).
40. T. Osaka, T. Hirano, Y. Sano, Y. Inubushi, S. Matsuyama, K. Tono, T. Ishikawa, K. Yamauchi, and M. Yabashi, "Wavelength-tunable split-and-delay optical system for hard x-ray free-electron lasers," Opt. Express **24**(9), 9187–9201 (2016).
41. T. Osaka, T. Hirano, Y. Morioka, Y. Sano, Y. Inubushi, T. Togashi, I. Inoue, K. Tono, A. Robert, K. Yamauchi, J. B. Hastings, and M. Yabashi, "Characterization of temporal coherence of hard X-ray free-electron laser pulses with single-shot interferograms," IUCrJ **4**(6), 728–733 (2017).
42. H. Li, Y. Sun, J. Vila-Comamala, T. Sato, S. Song, P. Sun, M. H. Seaberg, N. Wang, J. B. Hastings, M. Dunne, P. Fuoss, C. David, M. Sutton, and D. Zhu, "Generation of highly mutually coherent hard-x-ray pulse pairs with an amplitude-splitting delay line," Phys. Rev. Res. **3**(4), 043050 (2021).
43. A. V. Zozulya, A. Shabalin, H. Schulte-Schrepping, J. Heuer, M. Spiwek, I. Sergeev, I. Besedin, I. A. Vartanyants, and M. Sprung, "Wavefront preserving channel-cut optics for coherent x-ray scattering experiments at the P10 beamline at PETRAIII," J. Phys.: Conf. Ser. **499**, 012003 (2014).
44. X. Shi, R. Dinapoli, B. Henrich, A. Mozzanica, B. Schmitt, R. Mazzocco, H. Krüger, U. Trunk, and H. Graafsma, "Challenges in chip design for the AGIPD detector," Nucl. Instrum. Methods Phys. Res., Sect. A **624**(2), 387–391 (2010).
45. D. Mezza, A. Allahgholi, G. Arino-Estrada, L. Bianco, A. Delfs, R. Dinapoli, P. Goettlicher, H. Graafsma, D. Greiffenberg, H. Hirsemann, S. Jack, R. Klanner, A. Klyuev, H. Krueger, A. Marras, A. Mozzanica, J. Poehlsen, B. Schmitt, J. Schwandt, I. Sheviakov, X. Shi, U. Trunk, Q. Xia, J. Zhang, and M. Zimmer, "Characterization of AGIPD1.0: The full scale chip," Nucl. Instrum. Methods Phys. Res., Sect. A **838**, 39–46 (2016).
46. D. Mezza, A. Allahgholi, A. Delfs, R. Dinapoli, P. Goettlicher, H. Graafsma, D. Greiffenberg, H. Hirsemann, A. Klyuev, T. Laurus, A. Marras, A. Mozzanica, I. Perova, J. Poehlsen, B. Schmitt, I. Sheviakov, X. Shi, U. Trunk, Q. Xia, J. Zhang, and M. Zimmer, "New calibration circuitry and concept for AGIPD," J. Instrum. **11**(11), C11019 (2016).
47. A. J. F. Siegert, "On the fluctuations in signals returned by many independently moving scatters," Report **No. 465** (Radiation laboratory, Massachusetts Institute of Technology, 1943).
48. D. Ferreira, R. Bachelard, W. Guerin, R. Kaiser, and M. Fouché, "Connecting field and intensity correlations: The siegert relation and how to test it," Am. J. Phys. **88**(10), 831–837 (2020).
49. J. Möller, M. Sprung, A. Madsen, and C. Gutt, "X-ray photon correlation spectroscopy of protein dynamics at nearly diffraction-limited storage rings," IUCrJ **6**(5), 794–803 (2019).
50. F. Lehmkühler, W. Roseker, and G. Grübel, "From femtoseconds to hours—measuring dynamics over 18 orders of magnitude with coherent x-rays," Appl. Sci. **11**(13), 6179 (2021).
51. P. K. Dixon and D. J. Durian, "Speckle visibility spectroscopy and variable granular fluidization," Phys. Rev. Lett. **90**(18), 184302 (2003).
52. C. DeCaro, V. N. Karunaratne, S. Bera, L. B. Lurio, A. R. Sandy, S. Narayanan, M. Sutton, J. Winans, K. Duffin, J. Lehuta, and N. Karonis, "X-ray speckle visibility spectroscopy in the single-photon limit," J. Synchrotron Radiat. **20**(2), 332–338 (2013).
53. J. Goodman, *Speckle Phenomena in Optics: Theory and Applications* (Roberts & Company, 2007).
54. K. H. Kim, A. Späh, H. Pathak, F. Perakis, D. Mariedahl, K. Amann-Winkel, J. A. Sellberg, J. H. Lee, S. Kim, J. Park, K. H. Nam, T. Katayama, and A. Nilsson, "Maxima in the thermodynamic response and correlation functions of deeply supercooled water," Science **358**(6370), 1589–1593 (2017).
55. M. Leitner, B. Sepiol, L.-M. Stadler, B. Pfau, and G. Vogl, "Atomic diffusion studied with coherent x-rays," Nat. Mater. **8**(9), 717–720 (2009).
56. A. Girelli, H. Rahmann, N. Begam, A. Ragulskaya, M. Reiser, S. Chandran, F. Westermeier, M. Sprung, F. Zhang, C. Gutt, and F. Schreiber, "Microscopic dynamics of liquid-liquid phase separation and domain coarsening in a protein solution revealed by x-ray photon correlation spectroscopy," Phys. Rev. Lett. **126**(13), 138004 (2021).